Measurement of the N to Δ Transition Form Factors with the SoLID detector

A Jefferson Lab Letter of Intent to PAC 51

M. Paolone (spokesperson)[1]
New Mexico State University, Las Cruces, NM, USA

H. Atac (spokesperson), N. Sparveris (spokesperson)
Temple University, Philadelphia, PA 19122, USA

[1] contact:mpaolone@nmsu.edu

Executive Summary

Main Physics Goals: The Letter of Intent focuses on the measurement of the $N \rightarrow \Delta$ transition form factors (TFFs) at high Q^2, within the kinematic range accessible to the SoLID detector in a standard configuration.

Proposed Measurement: Using the SoLID detector in its "J/ψ" configuration, cross section measurements at the $\Delta(1232)$ resonance region for the $H(e,e'p)\pi^\circ$ reaction will be made for Q^2 between 5.0 to 8.0 (GeV/c)^2 and for the $H(e,e'\pi^+)n$ reaction for Q^2 between 2.0 to 8.0 (GeV/c)^2. The experiment will acquire production data parasitically during the SoLID "J/ψ" production running of 50 + 10 days. The TFFs will be extracted from fits to the cross section over the SoLID detector acceptance. The proposed future energy upgrade at JLab will allow to extend further the physics reach of these measurements beyond $Q^2 \sim 20$ (GeV/c)^2.

Specific requirements on detectors, targets, and beam: The experiment will be run parasitically with E12-12-006 with the addition of a trigger configuration for the proposed channels. The E12-12-006 target is a 15 cm LH2 cell which sits upstream from the SIDIS target center by 10 cm. The detector standard detector package for the J/ψ configuration includes the standard GEM planes, forward and large angle SPD, MRPC, forward and large angle EC, and both light and heavy gas Cherenkov detectors.

Abstract

The first excited state of the nucleon dominates many nuclear phenomena at energies above the pion-production threshold and plays a prominent role in the physics of the strong interaction. The study of the $N \rightarrow \Delta$ transition form factors (TFFs) in particular, sheds light on key aspects of the nucleonic structure that are essential for a complete understanding of nucleon dynamics. Here we propose a set of pion electro-production measurements in the first nucleon resonance, that can be conducted in-parallel (parasitic) to the SoLID J/ψ experiment. The proposed measurements will allow the precise extraction of the $N \rightarrow \Delta$ TFFs within a sparsely measured kinematic region, will improve significantly the precision of the world-data, and will provide stringent constraints and guidance towards improved theoretical calculations that focus on the pQCD regime. Possibilities for additional measurements, should the proposed energy upgrade at JLab become reality, will allow to extend significantly the physics reach of this research program in the future beyond Q^2 values of $20(GeV/c)^2$ in tandem with the SoLID setup.

1 Introduction and physics motivation

The first excited state of the nucleon holds a central role in the physics of the strong interaction. It dominates many nuclear phenomena at energies above the pion-production threshold, providing a path to gain insight to key aspects of the nucleonic structure through the experimental and theoretical exploration of the transition form factors. Historically, a main motivation of these studies during the early stages of this physics program involved the understanding of the underlying dynamical mechanisms in the nucleon that were responsible for the presence of non-spherical components in the nucleon wavefunction. Since hadrons are composite systems with complex quark-gluon and meson cloud dynamics, they give rise to non-spherical components in their wavefunction, which in a classical limit and at large wavelengths will correspond to a "deformation"[1–4]. Understanding the shapes of the fundamental building blocks in nature has always been a particularly fertile line of investigation for the understanding of the interactions of their constituents amongst themselves and the surrounding medium. In the case of hadrons this involves the highly non-linear interquark interaction and the quark-gluon dynamics. For the proton, the vanishing of the spectroscopic quadrupole moment, due to its spin 1/2 nature, precludes access to the most direct observable of deformation. Consequently, the presence of the resonant quadrupole amplitudes $E_{1+}^{3/2}$ and $S_{1+}^{3/2}$ (or E2 and C2 photon absorption multipoles respectively) in the predominantly magnetic dipole $M_{1+}^{3/2}$ (or M1) $\gamma^* N \to \Delta$ transition emerged as the most direct experimental signature for such an effect[1–43]. The relative strength of the $E2$ and $C2$ amplitudes is normally quoted in terms of their ratio to the dominant magnetic dipole, namely through the EMR and CMR ratio respectively. Nonvanishing quadrupole amplitudes will signify that either the proton or the $\Delta^+(1232)$ (or more likely both) are characterized by non-spherical components in their wavefunctions. The transition form factors (TFFs) have been explored up to four momentum transfer squared $Q^2 = 6\ (GeV/c)^2$ [8–16, 16–24, 30–36] (see Fig. 1) and the experimental results are in reasonable agreement with models invoking the presence of non-spherical components in the nucleon wavefunction.

Starting with the constituent-quark picture of hadrons, the quadrupole TFFs are a consequence of the non-central, color-hyperfine interaction among quarks[2,6]. Nevertheless, this mechanism can only provide a small fraction of the observed quadrupole signal at low momentum transfers, with the magnitudes of this effect for the predicted E2 and C2 amplitudes[7] being at least an order of magnitude too small to explain the experimental results and with the dominant M1 matrix element being $\approx 30\%$ low. A likely cause of these dynamical shortcomings is that such quark models do not respect chiral symmetry, whose spontaneous breaking leads to strong emission of virtual pions (Nambu-Goldstone Bosons)[5]. These couple to nucleons as $\vec{\sigma} \cdot \vec{p}$ where $\vec{\sigma}$ is the nucleon spin, and $\vec{p}$ is the pion momentum. The coupling is strong in the p wave and mixes in non-zero angular momentum components. Based on this, it is physically reasonable to expect that the pionic contributions increase the M1 and dominate the E2 and C2 transition matrix elements in the low Q^2 (large distance) domain. This was first indicated by adding pionic effects to quark models[37–39], subsequently in pion cloud model calculations[26,27], and recently demonstrated in Chiral Effective Field Theory calculations[40].

The TFFs have so far been widely studied, particularly at the low and intermediate momentum transfers, allowing significant progress towards our understanding of key aspects of the nucleon dynamics[4]. A wide spectrum of theoretical calculations for the TFFs is shown in Fig. 2. The challenge now lies towards a new generation of experimental measurements, of higher precision and of extended kinematic reach, that in tandem with refined theoretical calculations will enable the in-depth understanding of the system dynamics, and will allow a more complete picture of the interplay of the relevant degrees-of-freedom in the proton as one transitions from the low to the high energy scale within the system. The recently approved E12-22-001 experiment in Hall C will focus on the low momentum transfer region, targeting the mesonic

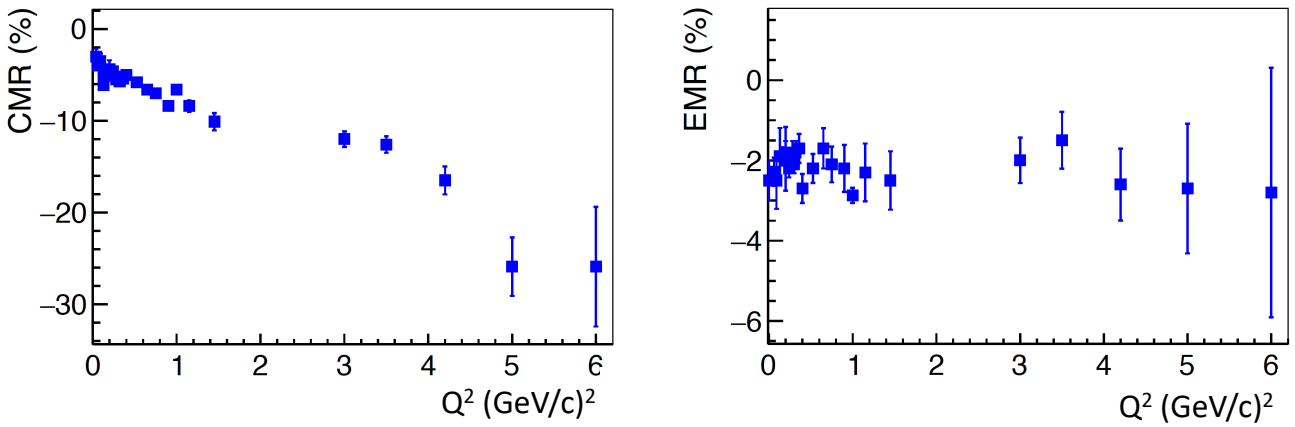

Figure 1. The world data[8–16, 16–24, 30–36] for the CMR and the EMR ratios.

cloud dynamics that is predicted to be dominant and rapidly changing within the experiment kinematics, offering a test bed for chiral effective field theory calculations. The experiment will allow to test the theoretical prediction that the Electric and the Coulomb quadrupole amplitudes converge as $Q^2 \to 0$ (see Fig. 2). In this Letter-of-Intent, we aim to complement this physics program with measurements that will target the high momentum transfer region. The proposed measurements will allow to understand the role of the effective degrees of freedom as we transition from the low to high energies, will provide benchmark data for state-of-the-art lattice QCD calculations that are currently in the works, and will allow to test another important prediction of pQCD, namely that EMR$\to$1 at high momentum transfers. This prediction is at the moment contradicted from the world-data that span a kinematic region up to $Q^2 = 6\ GeV^2$. The proposed measurements will add to the world-data, they will improve their precision and extend the range of Q^2 to 8.0 GeV^2, while the proposed energy upgrade at JLab in tandem with the SoLID detector opens a unique door to extend the reach for the TFFs past $Q^2 = 20\ GeV^2$. The scientific benefit of the proposed measurements can extend further to a wide range of timely scientific fronts (e.g. from hadronic to neutrino physics) where the TFFs enter as an input, as discussed in the next section.

2 Theoretical descriptions of the $\gamma^* N\Delta$ transition

Working on the basis of the symmetries of QCD and its large number-of-color (N_c) limit, where the baryon sector formed of up, down, and strange quark flavors displays an $SU(6)$ spin-flavor symmetry, one can achieve a first theoretical description of the predominantly magnetic dipole ($M1$) $\gamma^* N\Delta$ transition. The spin-flavor global symmetry of QCD is at the foundation of many quark models, in which baryons are described as non-relativistic quantum-mechanical three-quark system moving in a confining potential. Within that context, the $N \to \Delta$ transition is described by an $M1$ spin flip of a quark in the S-wave state. The SU(6) symmetry allows to relate the magnetic dipole moments of the proton and the $p \to \Delta^+$ transition as $\mu_{p\to\Delta^+} = 2\sqrt{2}/3\,\mu_p = 2.63\,\mu_N$, that falls somewhat short compared to the experimentally derived[48] $\mu_{p\to\Delta^+} = [3.46 \pm 0.03]\,\mu_N$. A D-wave admixture in the nucleon or the Δ wave functions on the other hand, allows for non-zero values in the $E2$ and $C2$ quadrupole transitions.

In the early quark model of Isgur-Karl[49] the constituent quarks move in a harmonic oscillator type long-range confining potential, which is supplemented by an interquark force corresponding with one-gluon exchange. This one-gluon exchange leads to a color hyperfine interaction - which was found to predict well the mass splittings between octet and decuplet baryons[50] - and contains a tensor force which produces

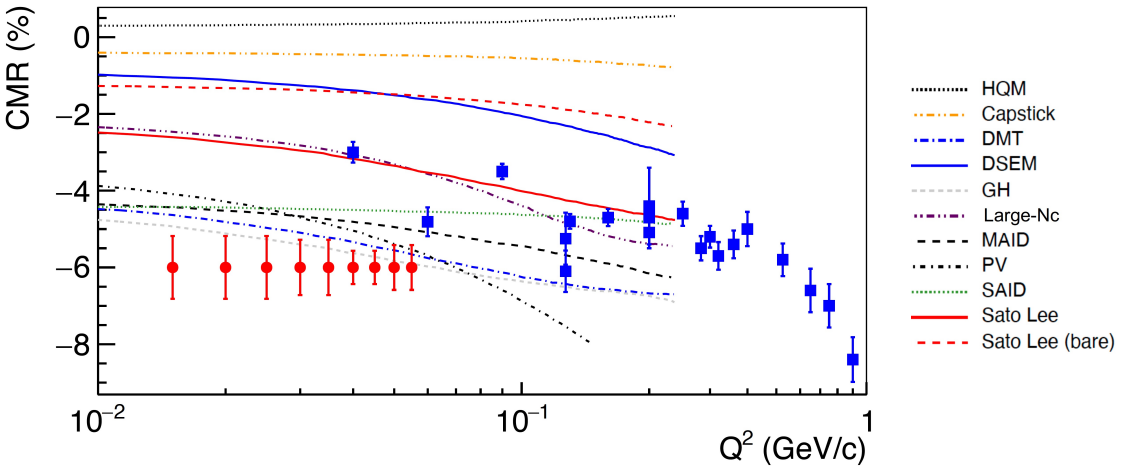

Figure 2. The theoretical predictions of MAID[28,44], DMT[27], SAID[45], PV[40], Sato-Lee[26], GH[41], Large-Nc[46], DSEM[47], Capstick[7] and HQM[42]. The world data (blue points) along with the projected measurements from E12-22-001 (red points) are also shown.

a D-state admixture in the N and Δ ground states of about 1 % [51,52]. As a consequence of such D-wave components, the N and Δ charge densities become non-spherical, resulting to small negative values in the sub-percent level for the EMR. Despite the success of the simplistic constituent quark model in predicting the structure and spectrum of low-lying baryons, it under-predicts $\mu_{N\to\Delta}$ by about 25 % and accounts for an EMR amplitude that is smaller by an order of magnitude compared to the experimental values. As a general consideration, the constituent quark models do not satisfy the symmetry properties of the QCD Lagrangian. The *chiral symmetry* is spontaneously broken in nature leading to the appearance of massless Goldstone modes (pions) which acquire a mass due to the explicit breaking of chiral symmetry. Being the lightest hadrons, the pions dominate the long-distance behavior of hadron wave functions and become particularly relevant in the $\Delta(1232)$ resonance that decays dominantly into πN. As such, a logical step is to include pionic degrees of freedom in order to qualitatively improve on the constituent quark models. Such efforts to integrate pionic effects in the N-Δ transition involved e.g. the chiral bag model[53,54], the Skyrme models[55,56], where the nucleon appears as a soliton solution of an effective non-linear meson field theory, the chiral quark soliton model (χQSM), which interpolates between a constituent quark model and the Skyrme model[57], etc. Other efforts based on quark models have restored chiral symmetry by including two-body exchange currents between the quarks, that lead to non-vanishing $\gamma^* N\Delta$ quadrupole amplitudes[58] even if the quark wave functions have no D-state admixture. In this type of hybrid quark & pion cloud models the non-zero values of the intrinsic quadrupole moments arises purely from the pion cloud. In the model of[58] the Δ is excited by flipping the spins of two quarks resulting to an EMR $\simeq -3.5\%$. The model also relates the $N\to\Delta$ and Δ^+ quadrupole moments to the neutron charge radius as $Q_{p\to\Delta^+} = r_n^2/\sqrt{2}$ and $Q_{\Delta^+} = r_n^2$. Using the experimental value for the neutron charge radius one derives from the above relation $Q_{p\to\Delta^+} = -0.08$ fm^2 that agrees well with the extracted value[48] for $Q_{p\to\Delta^+}$.

Aiming at results that are more directly related to QCD, one can follow theoretical approaches such as the $1/N_c$ expansion of QCD (limit of large number of colors), chiral effective field theory (chiral limit of small pion masses or momentum transfers) or lattice QCD simulations (continuum limit). The $1/N_c$ expansion of QCD[59,60] offers an expansion with a perturbative parameter at all energy scales and has proved quite useful in describing properties of baryons, such as, ground-state and excited masses, magnetic

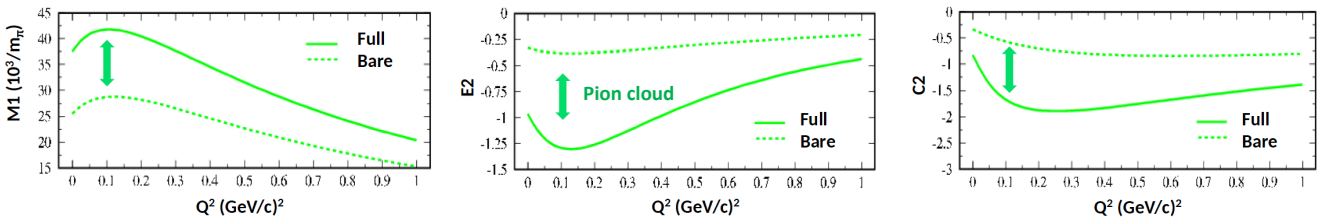

Figure 3. The effect of the pion cloud to the resonant amplitudes as predicted by the Sato Lee calculation (Bare: without the pion cloud).

moments, and electromagnetic decays[61,62]. For the $N \to \Delta$ transition, the magnetic moment $\mu_{N\to\Delta}$ is related to the isovector nucleon magnetic moment as[63] $\mu_{p\to\Delta^+} = (\mu_p - \mu_n)/\sqrt{2} \simeq 3.23\,\mu_N$ that agrees within 10 % of the experimentally derived value and the EMR value is shown to be of order $1/N_c^2$[64] thus offering a physical explanation of its magnitude in the large N_c limit. The relation $Q_{p\to\Delta^+} = r_n^2/\sqrt{2}$ that was discussed above was also shown[65] to hold in the large N_c limit. Furthermore in the large N_c limit it was shown[66] that at $Q^2 = 0$ the EMR $= (1/12)\, R_{N\Delta}^{3/2}\, (M_\Delta^2 - M_N^2) r_n^2/\kappa_V$ where $R_{N\Delta} \equiv M_N/M_\Delta$, and $\kappa_V = \kappa_p - \kappa_n$ is the isovector nucleon anomalous magnetic moment. The large N_c prediction yields EMR $= -2.77\,\%$ that is in excellent agreement with the experimental measurement for EMR. In the case of CMR, where a direct measurement at the real-photon point is not possible, extending the large-N_c relation to finite Q^2 leads to relations with the neutron electric form factor, which agree remarkably well with the experimental measurements[66,67].

Lattice QCD offers a direct path to calculate the N to Δ transition form factors starting from the underlying theory of QCD. The LQCD calculations[25,68] have been preformed so far with pion mass down to $\sim 300\ MeV$, where the Δ is still stable. These results tend to somewhat underestimate the M1, similarly to what has been observed in results for the nucleon EM form factors. Such effects can be further investigated through lattice calculations with smaller pion masses. The LQCD results for EMR and CMR on the other hand exhibit remarkable agreement with the experimental measurements, pointing to the fact that the ratios are much less affected by lattice artifacts than each of the quantities separately. The statistical uncertainties of the early LQCD results for the two ratios are somewhat large due to the fact that the two quadrupole amplitudes are sub-dominant and more challenging to determine. Nevertheless, recent progress enables most LQCD calculations to be conducted with physical pion mass, and with statistical uncertainties that are comparable to the experimental ones, thus making the need for new experimental measurements timely and extremely important. More specifically, the Δ-resonance is currently being investigated by the Extended Twisted mass Collaboration[69] using such gauge ensembles within the Luscher approach[70]. Calculations focusing on the Δ-resonance will be the next target using the same formalism developed for rho-meson[71] with the expectation that in the next couple of years lattice calculations of the transition form factors will emerge with much better controlled systematics. In Fig. 4 Lattice QCD results offer geometrical insight to the nucleon through calculations of the three-dimensional contour plot of the Δ^+[72] and of the Δ^+ quark transverse charge density[73].

A firm theoretical framework to approach the physics of interest at low scales involves the chiral effective field theory (χEFT), that allows the relevant symmetries of QCD to be built in consistently in the calculations. The N to Δ transition presents a challenge for χEFT as it involves the interplay of two light mass scales, the pion mass and the $N-\Delta$ mass difference. Studies, taking into account these two mass scales, have been performed within the framework of heavy-baryon chiral perturbation theory[74] or the more comprehensive study carried out[75,76] using the "ε-expansion" scheme. In the latter, the two

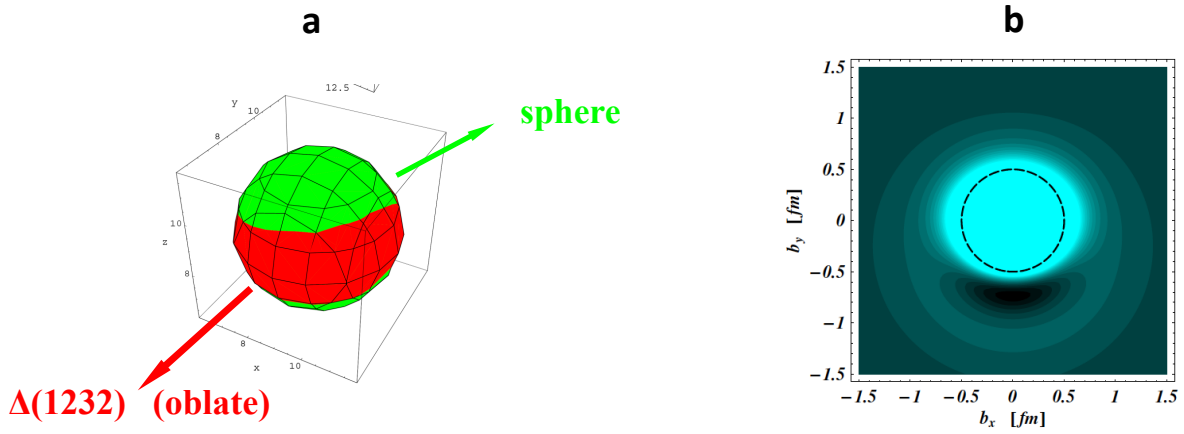

Figure 4. Lattice QCD results of the three-dimensional contour plot of the Δ^+[72] and of the Δ^+ quark transverse charge density[73].

scales, the pion mass $\varepsilon \equiv m_\pi/\Lambda_{\chi\text{SB}}$ (with $\Lambda_{\chi\text{SB}} \sim 1$ GeV the chiral symmetry breaking scale) and the Δ-resonance excitation energy $\delta \equiv (M_\Delta - M_N)/\Lambda_{\chi\text{SB}}$ are counted as being of the same order, namely $\varepsilon \sim \delta$. The "δ-expansion" scheme has been introduced[77] to provide an energy-dependent power-counting scheme that takes into account the large variation of the Δ-resonance contributions with energy, and treats the two light scales ε and δ on a different footing, counting $\varepsilon \sim \delta^2$, the closest integer-power relation between these parameters in the real world. It has been applied to the study of the N to Δ transition form factors[78] and has been used to extrapolate the current lattice QCD calculations to the physical pion mass, reconciling the lattice results and the experimental values for the CMR.

The measurement of the $N \to \Delta$ TFFs allows a powerful link between the underlying dynamics of the nucleon (as seen e.g. in Fig. 3) and the spatial representation of the transition charge density which induces the $N \to \Delta$ excitation[79], as viewed from a light front moving towards a transversely polarized nucleon. This transition charge density contains both monopole, dipole and quadrupole patterns. The quadrupole pattern shown in Fig. 5 maps the spatial dependence in the deformation of the transition charge distribution. The measurements proposed in this work will extend the TFF word-data measurements in the intermediate and high Q^2 region, and they will further improve upon their precision, thus allowing to extract the transition charge distributions with an unprecedented precision.

The scientific merit of the proposed measurements can be further identified through valuable input that the TFF measurements bring in a variety of timely scientific topics. Here we can refer to a couple of such examples. In one such case, that is directly related to the nucleon structure, the TFFs enter as input parameters in the measurement of the electromagnetic Generalized polarizabilities (GPs)[80,81] of the proton. The GPs characterize the proton's response to an external electric or magnetic field, and describe how easily the charge and magnetization distributions in the nucleon are distorted by the EM field as a function of the distance scale within the system. As the polarizabilities are sensitive to the excited spectrum of the nucleon, it becomes particularly beneficial to conduct the GPs measurements in the nucleon resonance where the signal is amplified (as opposed e.g. to measurements in the pion production threshold region). In extracting the GPs from the experimental measurements in the Δ region, the analysis of the VCS cross section measurements is conducted in the context of Dispersion Relations[82–84], where the transition form factors enter as an input. The accurate description of the TFFs becomes thus important for the precise extraction of the proton GPs[80,81]. In another example, that extends well beyond the

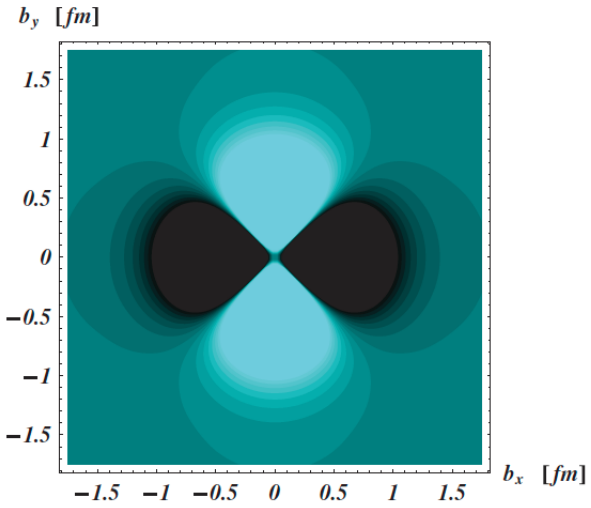

Figure 5. Quadrupole contribution to the transverse charge density for the $N \to \Delta$ transition[79], when N and Δ are polarized along the x axis with spin projection +1/2.

strict boundaries of the nucleon structure, the relevance of the Δ-resonance reaches out to neutrino oscillation experiments that focus on the study of the neutrino mass hierarchy and of the leptonic CP violation. The precise interpretation of these data requires a reliable understanding of neutrino-nucleus reactions[85,86], since the neutrinos are identified through the remnants of these reactions. The neutrino energy relevant to the oscillation experiments spans from several hundred MeV to a few GeV. This requires that the neutrino-nucleus reactions are well understood over a wide kinematical region where the dominant reaction mechanisms tend to vary across the quasi-elastic, resonance and deep inelastic regions. For relatively low energy neutrinos at the ~ 1 *GeV* range the Δ-resonance becomes particularly important. During the process, the internal structure of a scattered nucleon is excited to a resonant state that in-turn decays into a meson-baryon final state, where the meson-baryon dynamics play a central role. In extracting the neutrino properties from the experimental measurements, a dominant source of systematic error involves the uncertainties in neutrino-nucleus reaction cross sections. These contributions have to be understood with an accuracy at the few percent level in order to meet the objectives of the neutrino oscillation experiments. In addressing these uncertainties and reducing them to the desired level, a synergistic effort is required that combines precise experimental measurements in the Δ-resonance, nuclear theorists and neutrino experimentalists. One can continue with more examples, such as the relation[66,87,88] between the TFFs and the elastic form factors of the nucleon (e.g. see Fig. 6), that illustrate further the wealth and scientific potential associated with the measurements of interest.

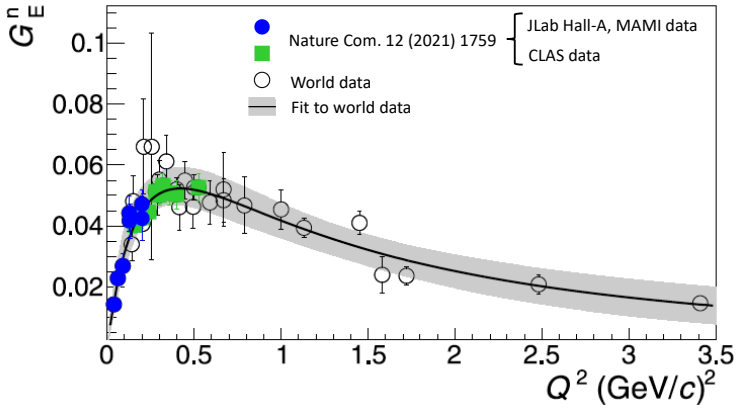

Figure 6. The world data for G_E^n are shown as open symbols. The extraction of G_E^n from the experimental measurements of the $N \rightarrow \Delta$ transition form factors[87] is shown with the filled (blue, green) symbols.

3 The Experiment

The proposed experiment will leverage the SoLID detector's high luminosity and 2π azimuthal acceptance to scan θ_{cm} and ϕ_{cm} bins of the recoil nucleon/pion over a W range centered at the $\Delta(1232)^+$ pole mass and over a range of intermediate to high Q^2 values. Since the expected cross-sections drop roughly exponentially with Q^2, two-arm spectrometer measurements become uneconomical in Hall-A/C. The CLAS12 collaboration has a program to explore Nucleon Resonances at 11 GeV (see PAC34 proposal PR-12-09-003[89] and PAC35 update: PR-12-09-003 update[90]) with single pion production coverage up to Q^2 = 12 GeV2, but the exact precision of an EMR and CMR extraction at the Delta resonance are not well detailed. This experiment will utilize the standard J/ψ setup for the SoLID detector (see PR-12-12-006[91]) and can be run parasitically with the addition of a trigger specific to the channels and kinematic settings described below. From these data, the transition form factors EMR and CMR can be extracted.

3.1 Experimental apparatus and set-up

Our proposed measurement of H(e,e'p)π^0 and H(e,e'π^+)n will require a single coincidence trigger, and will directly utilize the existing SoLID J/ψ setup, described here: The standard Hall A 15cm liquid Hydrogen target will be located upstream at $z = -10$ *cm* relative to the target center of the SoLID-SIDIS setup. The layout of the experiment is shown in Fig. 7. The detector system consists of forward and large angle detectors. With a polar angle coverage from 8° to 15°,the forward angle detectors can identify charged particles with momenta ranging from 0.8 GeV to 7.0 GeV. Particle tracking in the forward angle region is provided by 5 layers of GEM detectors. The particle identification will be obtained from a combination of an electromagnetic calorimeter(EC),a gas Cerenkov counter(GC),and a layer of Multi-gap Resistive Plate Chamber(MRPC). The polar angle coverage for the large angle detectors is from 15° to 25°. The large angle detectors can detect electrons and protons with momentum above 2.5 GeV. The particle identification will be achieved by an electromagnetic calorimeter.

3.2 Kinematical Settings

Four different kinematical settings are considered: Kin-p-SA (proton-π^0channel, small angle electron), Kin-p-LA (proton-π^0 channel, large angle electron), Kin-n-SA (neutron-π^+ channel, small angle electron), and Kin-n-LA (neutron-π^+ channel, large angle electron). For the proton kinematics, the proton is allowed to be detected over the full polar angle range of 8° to 25°. For both neutron kinematics, the π^+ is restricted

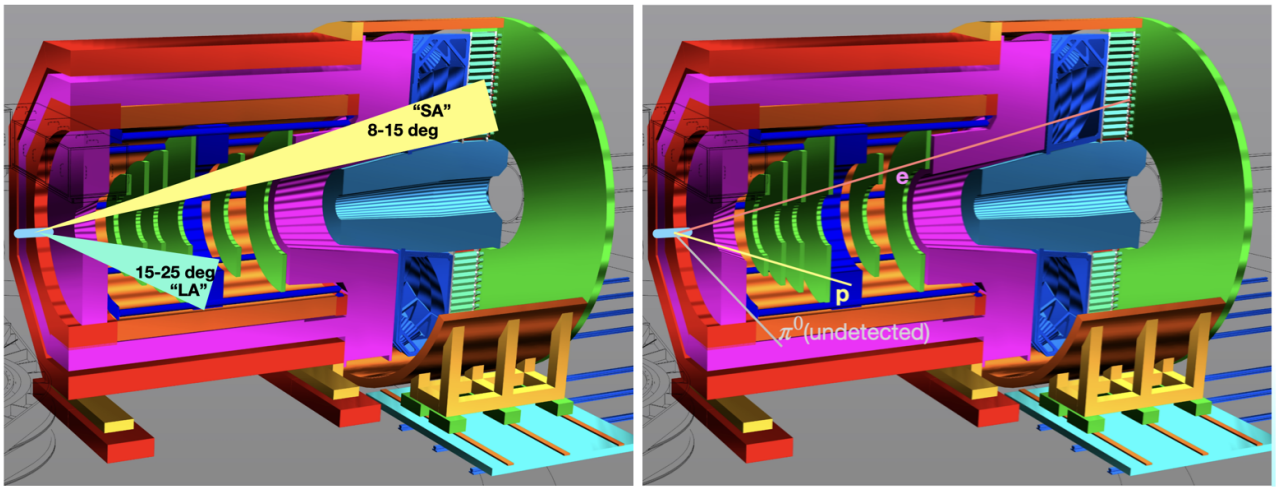

Figure 7. Left: The SoLID detector with the small-angle (SA) and large-angle (LA) acceptances. Right: Example of an Kin-p-SA event.

to the small angle coverage 15° to 25°, where the light gas Cherenkov is available for PID. for the SA/LA settings, the electron is either restricted to the small angle 8° to 15°, where the LGC can help with PID and the tracking resolutions are generally better, or allowed to be detected at large angle where only the large angle calorimeter provides PID.

The LA kinematics reach to generally higher Q^2 than the SA kinematics, and the neutron-π^+ channel can reach lower in Q^2 due to the detected π^+ having a more forward boost in the lab frame where the SoLID acceptance lies. Conversely, in the p-π^0 channel, the kinematics of the reaction force the proton mostly to the large-angle region. Fig. 7 shows the SoLID detector with a representation of the kinematics proposed.

As stated above, the resolution of the kinematic settings are different, which primarily affects the binning choices that are made for the cross-section extraction. The expected resolutions after tracking for Kin-p-SA and Kin-p-LA are shown in Fig. 8 and for Kin-n-SA and Kin-n-LA Fig.9.

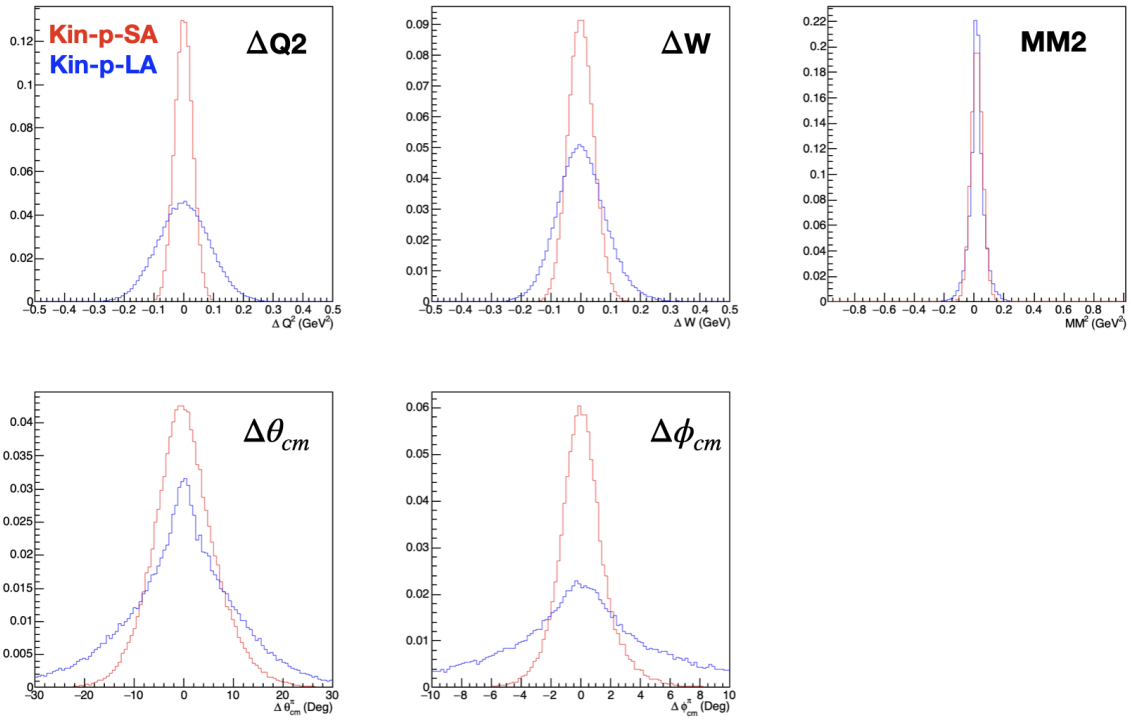

Figure 8. The expected resolutions of Kin-p-SA (red) and Kin-p-LA (blue) for (left to right, top to bottom): Q^2, W, M^2 of reconstructed missing particle, θ_{cm} of the pion, and ϕ_{cm} of the pion

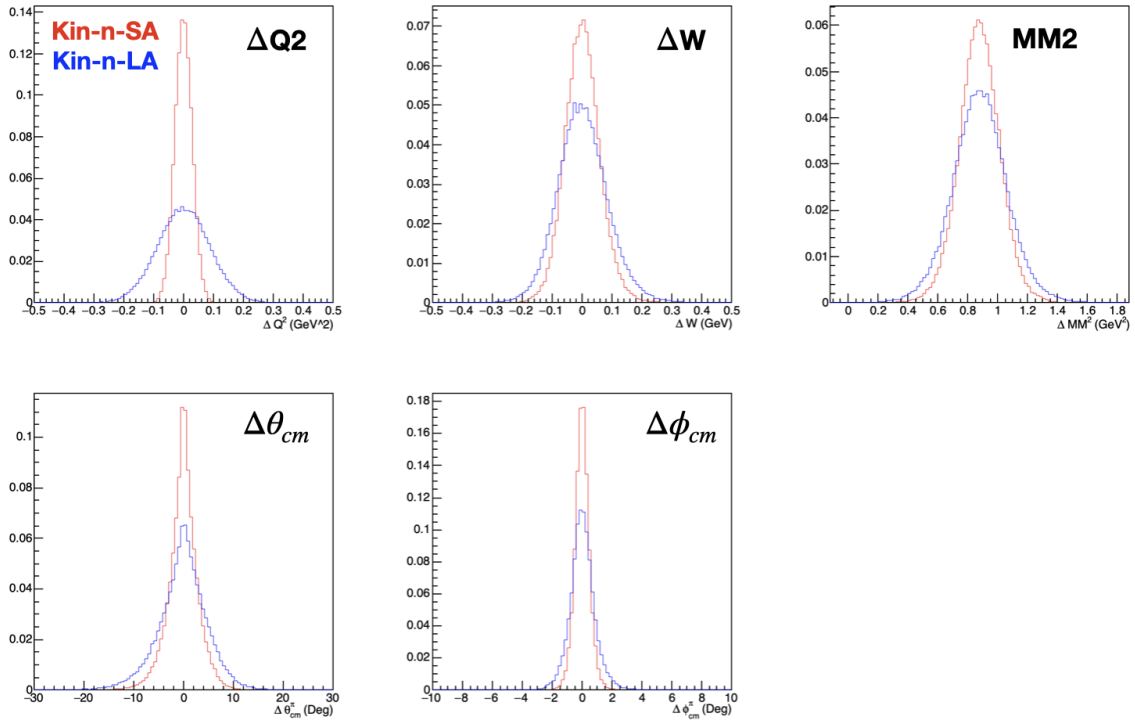

Figure 9. The expected resolutions of Kin-n-SA (red) and Kin-n-LA (blue) for (left to right, top to bottom): Q^2, W, M^2 of reconstructed missing particle, θ_{cm} of the pion, and ϕ_{cm} of the pion

3.3 Cross-section calculations and rate estimations

Few reliable models exist to produce cross-section calculations for $\Delta(1232)$ resonance pion production at large Q^2. The most commonly used MAID and SAID predictions are only available below $Q^2 = 5.0\ GeV^2$. For the purposes of rate estimation used in this letter, a simple exponential extrapolation has been used with the MAID model, fitting points between $Q^2 = 4.0\ -\ 5.0\ GeV^2$ at a fixed W, θ_{cm} and ϕ_{cm}. It is found, over the W, θ_{cm} and ϕ_{cm} considered in this experiment, that the MAID calculations follow very closely an exponential fall-off in Q^2 and present a reasonable estimation of the cross-sections at near Q^2 values. In the case where the SAID cross-section calculation is smaller than the MAID cross-section at exactly $Q^2 = 5.0\ GeV^2$, the final cross-section is scaled by the percentage deficit as a conservative estimation. An example of a an exponential fit used in the extrapolation is shown in Fig. 10.

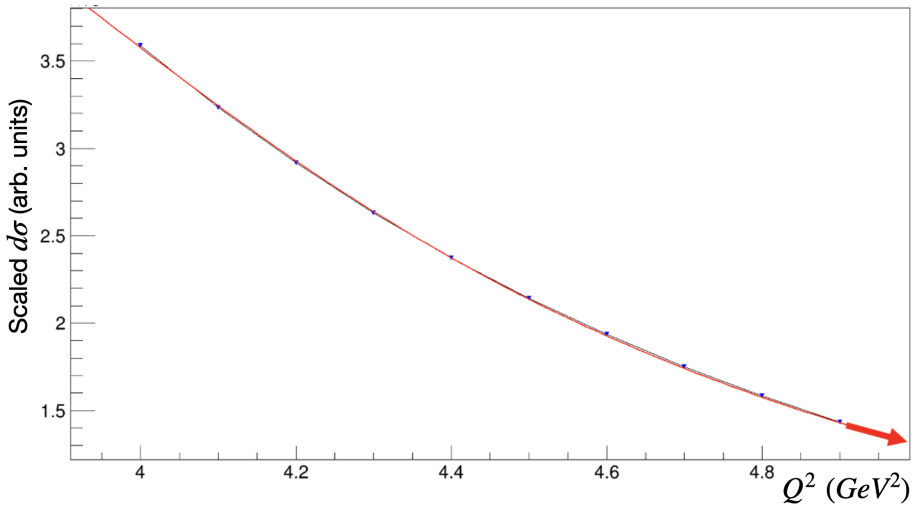

Figure 10. Example of the quality of fits to the MAID cross-section at fixed W, θ_{cm} and ϕ_{cm} to extrapolate to larger Q^2. Note: This fit is representative of the general quality of all the event-by-event fits used for the cross-section extrapolation in this experiment study.

At a given Q^2 and W, each multidimensional fit to extract the EMR and CMR must span some region of both θ_{cm} and ϕ_{cm}. The available phase-space to perform such a fit is dependent on the acceptance of the detector and as such is dependent on the kinematic setting being studied. Furthermore the expected resolutions per setting will impact both the bin-spacing and the expected systematic uncertainties of the cross-section extracted per bin. Shown in Fig. 11 are θ_{cm} and ϕ_{cm} plots binned in 10 deg increments over all possible angles for two Q^2 bins with a W bin of $1232\ \pm 30\ MeV$. The plot on the left is representative of the Kin-p-SA accepted phase-space with the plot on the right is representative of Kin-p-LA. The z-axis shows total rates in Hz for each expected bin. Note that the expected rates drop by an order of magnitude between $Q^2 = 5.7$ and $8.0\ GeV^2$ but the increase in available phase-space provides a lever-arm that generally improves the EMR and CMR extraction even as the total uncertainty per bin increases.

The expected accidental background has been calculated using full monte-carlo simulation of the detector. Per Q^2, W, and θ_{cm} and ϕ_{cm} bin, the predicted singles electron accidental rate is expected to peak on the order of 10 Hz before missing mass selection. The proton singles rates are then expected to be 0.5 kHz while the π^+ rates contribute 3.0 kHz. Assuming a conservative trigger width of 100 ns, the total accidentals rate should be maximally around 0.003 Hz which is on par with the rates expected per bin in lowest rate (highest Q^2) bins of the analysis. The maximum Q^2 bin considered in this letter ($Q^2 = 8.0$) is chosen by to keep the signal-to-backgrounds manageable and < 1.

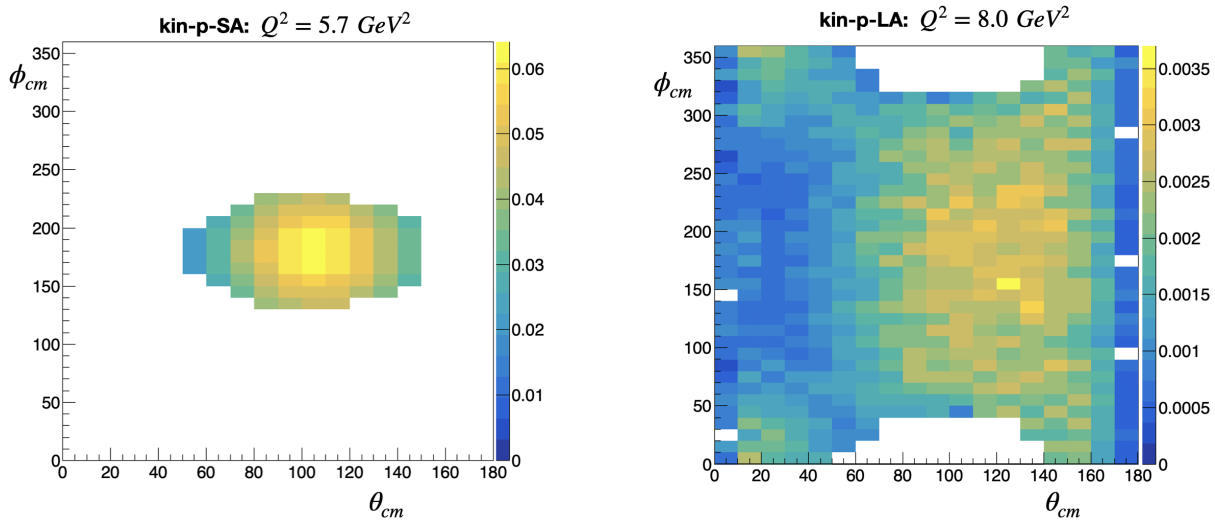

Figure 11. The θ_{cm} and ϕ_{cm} coverage versus expected signal rate (Hz) for 10 deg by 10 deg bins. Left: $Q^2 = 5.7\ GeV^2$ in Kin-p-SA. Right: $Q^2 = 8.0\ GeV^2$ in Kin-p-LA.

Systematic uncertainties on the cross-section normalization follow from the SoLID-J/ψ and SoLID-SIDIS studies in their respective proposals. The total systematic uncertainty on the two-particle coincidence measurements are expected to be of the order $\approx 5-7\%$ for small-angle electron kinematics and $\approx 10\%$ for the large angle electron kinematics. At most Q^2 below the highest value measured, the systematic uncertainty will dominate the total uncertainty on the cross-section.

Contributions from additional backgrounds are expected to be minimal. A cut on the W variable around the Δ mass does a good job of limiting production of higher mass mesons beyond the pion, or 2+ meson production. The $\Delta \rightarrow p + \gamma$ channel does exist, and the missing mass resolution is not expected to be good enough to separate the channels. However, by branching ratio alone, the VCS photon channel is 100 times less likely than the pion channel decay. The Bethe-Heitler contribution is not expected to significantly contribute in this region, but a more careful study of how BH processes may radiate into the acceptance need to be explored. Other single-pion backgrounds which are indistinguishable from the desired signal are taken into account by theoretical calculation and subtracted in the EMR and CMR extraction as discussed below.

3.4 Data analysis and projected results

The cross section of the $p(e,e'p)\pi^\circ$ reaction is sensitive to a set of independent partial responses $(\sigma_T, \sigma_L, \sigma_{LT}, \sigma_{TT})$:

$$\frac{d^5\sigma}{d\omega d\Omega_e d\Omega_{pq}^{cm}} = \Gamma(\sigma_T + \varepsilon\cdot\sigma_L - v_{LT}\cdot\sigma_{LT}\cdot\cos\phi_{pq}^* + \varepsilon\cdot\sigma_{TT}\cdot\cos 2\phi_{pq}^*)$$

where $v_{LT} = \sqrt{2\varepsilon(1+\varepsilon)}$ is a kinematic factor, ε is the transverse polarization of the virtual photon, Γ is the virtual photon flux, and ϕ_{pq}^* is the proton azimuthal angle with respect to the electron scattering plane. The differential cross sections $(\sigma_T, \sigma_L, \sigma_{LT}, \sigma_{TT})$ are all functions of the center-of-mass energy W, the Q^2, and the proton center of mass polar angle θ_{pq}^* that is measured from the momentum transfer direction. The $\sigma_0 = \sigma_T + \varepsilon\cdot\sigma_L$ response is dominated by the $M1$ resonant multipole while the interference of the $C2$ and $E2$ amplitudes with the $M1$ dominates the Longitudinal - Transverse and Transverse - Transverse responses, respectively. Cross section measurements will be performed at the nucleon resonance region,

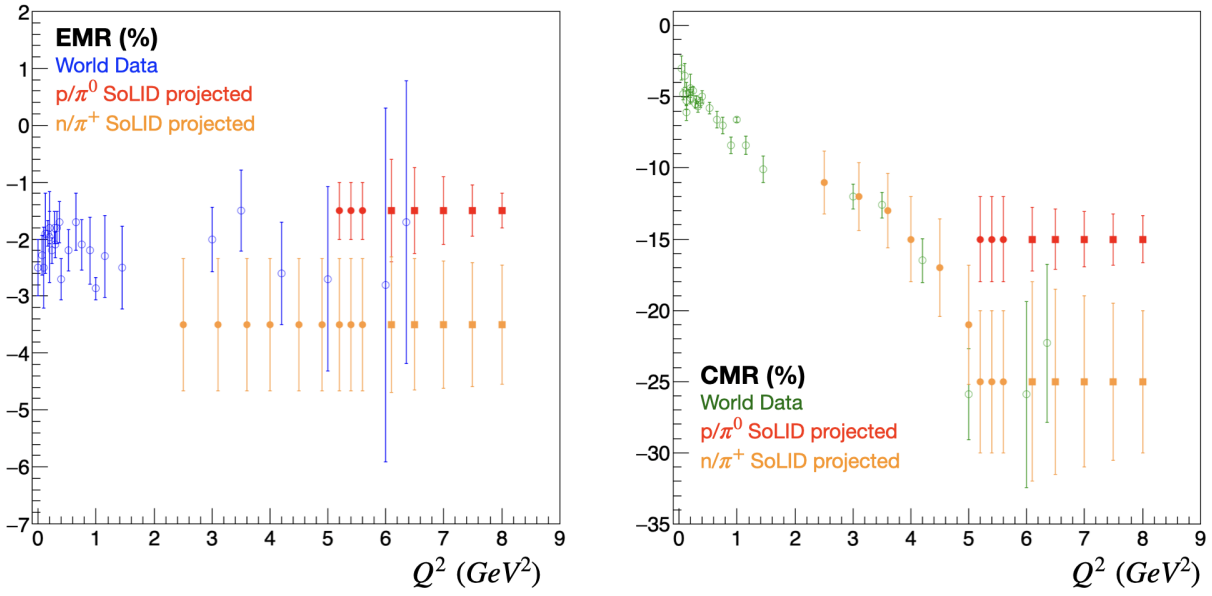

Figure 12. The projected CMR and EMR measurements along with world data. The overlapping Q^2 points between kinematic settings have been arbitrarily offset for better clarity.

extending from $Q^2 = 2\ (GeV/c)^2$ to $Q^2 = 5.5\ (GeV/c)^2$. Point cross sections will be extracted from the finite acceptances by utilizing the cross section calculations from the state of the art theoretical models[26–28,44,45] in the Monte Carlo simulation. Radiative corrections, energy losses and resolution effects will be integrated in the data analysis using the Monte Carlo simulation.

For the extraction of the resonant amplitudes from the measured cross sections, consideration has to be given in the treatment of the non-resonant pion electro-production amplitudes that interfere with the resonant amplitudes in the $N \rightarrow \Delta$ transition. These interfering contributions, small in magnitude but large in number, can not be sufficiently constrained by the experimental measurements, and they thus result into a model uncertainty for the quadrupole transition form factors. In the past these contributions have been occasionally poorly studied or quoted as an uncertainty. Here, the effect of these amplitudes is studied by employing in the data analysis state of the art theoretical pion electroproduction models[26–28,44,45]. Fits of the resonant amplitudes will be performed while taking into account the contributions of background amplitudes from the different models. The models offer different descriptions for the background amplitudes, leading to deviations in the extracted values of the transition form factors that are quantified as a model uncertainty. This procedure has been followed in the past in various experiments e.g.[21,23,31,36].

The projected measurements for the two transition form factors are shown in Fig. 12. The red-circles show projections from the kin-p-SA settings, red-squares are from Kin-p-LA, orange-circles are from kin-n-SA, and orange-squares are from Kin-n-LA. Points for the various kinematics have been offset on the y-axis for clearer comparisons.

3.5 Possibilities with a CEBAF energy upgrade

While not the primary focus of this letter, the Q^2 reach of the SoLID detector to measure the N-Delta transition form factors has been briefly explored. At the moment, the SoLID detector is expected to be permanent Hall-A detector after it is installed. Should Jefferson Lab see an energy upgrade, the SoLID detector would likely be already installed. The corresponding Q^2 reach for phase-space alone is shown in Fig. 13 for a 20 GeV beam at JLab. Not shown is that the θ_{cm} and ϕ_{cm} coverage becomes almost 4π and

even at low counting rates, the extent of the coverage may provide reasonable extractions of the EMR and CMR beyond $Q^2 = 10.0\ GeV^2$.

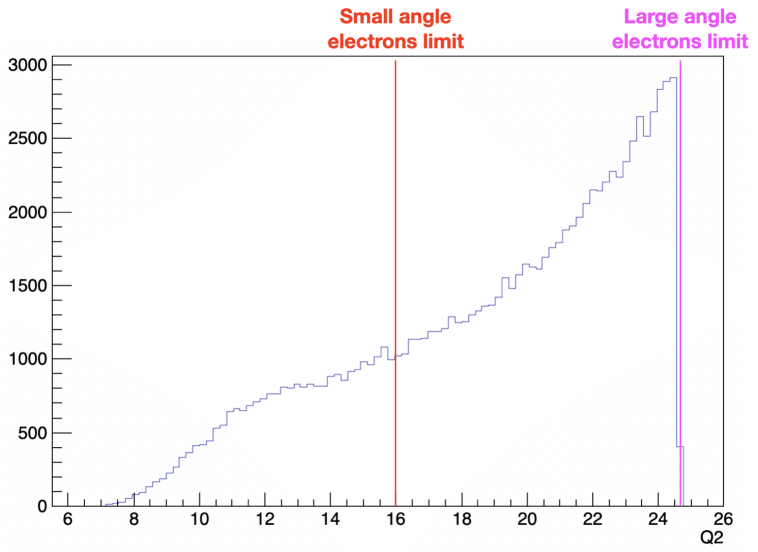

Figure 13. 20 GeV beam phase-space-only expected Q^2 coverage for N-Delta transition from factor extraction. The limits of the small-angle and large-angle extractions are shown by the vertical lines.

4 Summary

The first excited state of the nucleon holds a prominent role in the physics of the strong interaction and as such it has been a central part of Jefferson Lab's experimental program. In this work we will extend this physics program and we will explore key aspects of the nucleonic structure that are essential in order to decode the dynamics of the system. We will conduct a precise study of the mesonic cloud dynamics in a region where they are dominant and rapidly changing. We will perform measurements of the quadrupole TFFs that have emerged as the experimental signature for the presence of non-spherical components in the nucleon wavefunction, aiming to decode the underlying system dynamics, and will provide benchmark data that will offer a test bed for chiral effective field theory calculations and lattice QCD calculations. The proposed measurements will add valuable data to test to the pQCD predictions that the EMR $\rightarrow$ 1 and the CMR becomes constant at large Q^2. Beyond the direct benefit in our understanding of the baryon structure, the new data for the TFFs will serve as an input in a number of scientific topics ranging from the hadronic to neutrino physics, thus extending the impact and the scientific merit of the proposed measurements across different domains of nuclear and particle physics.

The experiment will require the standard J/ψ configuration of the SoLID detector and may run parasitically alongside the approved experiment with the addition of triggers to collect data in the kinematical settings presented above.

The SoLID collaboration review committee has endorsed this LOI on physics merit and experimental feasibility, but has made a list of items that need more consideration before a full proposal is brought to the PAC. Those items include:

- An exploration of additional comparisons beyond pQCD predictions at large Q^2, like direct lattice comparisons or even TFF GPD extractions.

- A better exploration of the data that will be available with the CLAS12 program, and the expected precision of EMR and CMR extractions from that program.
- Explore the benefits of a dedicated "N-Delta" setup with the SoLID detector, and what advantages might be gained by de-coupling the experimental settings from the J/ψ settings.
- Perform a more careful study of possible background channels and how they may radiate into the acceptance.
- For the largest Q^2 available, rate estimates become more critical. Explore other models for pion electroproduction at large Q^2 and compare extrapolations from MAID or SAID.

References

1. A. de Rujula, H. G. & Glashow, S. *Phys. Rev. D* **12**, 147 (1975).
2. Glashow, S. *Physica* **96A**, 27 (1979).
3. Bernstein, A. & Papanicolas, C. Shapes of hadrons. *AIP. Conf. Proc.* **904**, 1 (2007).
4. Alexandrou, C., Papanicolas, C. & Vanderhaeghen, M. *Rev. Mod. Phys.* **84**, 1231 (2012).
5. Bernstein, A. *Eur. Phys. J. A* **17**, 349 (2003).
6. N. Isgur, G. K. & Koniuk, R. *Phys. Rev.* **D25**, 2394 (1982).
7. Capstick, S. & Karl, G. *Phys. Rev.* **D41**, 2767 (1990).
8. Blanpied, G. *Phys. Rev. Lett.* **79**, 4337 (1997).
9. Beck, R. *et al. Phys. Rev. Lett.* **78**, 606 (1997).
10. Beck, R. *et al. Phys. Rev.* **C61**, 035204 (2000).
11. Frolov, V. *et al. Phys. Rev. Lett.* **82**, 45 (1999).
12. Pospischil, T. *et al. Phys. Rev. Lett.* **86**, 2959 (2001).
13. Mertz, C. *et al. Phys. Rev. Lett.* **86**, 2963 (2001).
14. Bartsch, P. *et al. Phys. Rev. Lett.* **88**, 142001 (2002).
15. van Buuren, L. *et al. Phys. Rev. Lett.* **89**, 012001 (2002).
16. van Buuren, L. *et al. Phys. Rev. C* **70**, 042201 (2004).
17. Kunz, C. *et al. Phys. Lett. B.* **564**, 21 (2003).
18. Sparveris, N. F. *et al.* Investigation of the conjectured nucleon deformation at low momentum transfer. *Phys. Rev. Lett.* **94**, 022003 (2005).
19. Kelly, J. *Phys. Rev. Lett.* **95**, 102001 (2005).
20. Kelly, J. J. *et al.* Recoil polarization measurements for neutral pion electroproduction at $Q^2 = 1$ $(GeV/c)^2$ near the Delta resonance. *Phys. Rev.* **C75**, 025201 (2007).
21. Stave, S. *et al.* Lowest Q^2 Measurement of the $\gamma*$ p —> Δ Reaction: Probing the Pionic Contribution. *Eur. Phys. J.* **A30**, 471–476 (2006).
22. Ungaro, M. *et al. Phys. Rev. Lett.* **97**, 112003 (2006).
23. Blomberg, A. *et al.* Electroexcitation of the $\Delta^+(1232)$ at low momentum transfer. *Phys. Lett.* **B760**, 267–272 (2016).
24. Blomberg, A. *et al.* Virtual Compton Scattering measurements in the nucleon resonance region. *Eur. Phys. J. A* **55**, 182 (2019). 1901.08951.
25. Alexandrou, C. *et al. Phys. Rev. Lett.* **94**, 021601 (2005).
26. Sato, T. & Lee, T. Dynamical study of the Delta excitation in N (e, e-prime pi) reactions. *Phys. Rev. C* **63**, 055201 (2001).
27. Kamalov, S. & Yang, S. N. Pion cloud and the Q^2 dependence of $\gamma*$ N <—> Δ transition form-factors. *Phys. Rev. Lett.* **83**, 4494–4497 (1999).
28. Kamalov, S., Chen, G.-Y., Yang, S.-N., Drechsel, D. & Tiator, L. Pi0 photoproduction and electroproduction at threshold within a dynamical model. *Phys. Lett. B* **522**, 27–36 (2001).

29. SAID. http://gwdac.phys.gwu.edu.

30. Elsner, D. *et al.* Measurement of the LT-asymmetry in π^0 electroproduction at the energy of the $\Delta(1232)$ resonance. *Eur. Phys. J.* **A27**, 91–97 (2006).

31. Sparveris, N. F. *et al.* Determination of quadrupole strengths in the $\gamma * p \to \Delta(1232)$ transition at $Q^2 = 0.20\ (GeV/c)^2$. *Phys. Lett.* **B651**, 102–107 (2007).

32. Stave, S. *et al. Phys. Rev. C* **78**, 024209 (2008).

33. Aznauryan, I. G. *et al.* Electroexcitation of nucleon resonances from CLAS data on single pion electroproduction. *Phys. Rev.* **C80**, 055203 (2009).

34. Villano, A. N. *et al. Phys. Rev. C* **80**, 035203 (2009).

35. van Buuren, L. *et al. Phys. Rev. C* **84**, 028201 (2011).

36. Sparveris, N. *et al.* Measurements of the γ*p $\to \Delta$ reaction at low Q^2. *Eur. Phys. J.* **A49**, 136 (2013).

37. D.-H. Lu, A. W. T. & Williams, A. G. *Phys. Rev. C* **55**, 3108 (1997).

38. U. Meyer, E. H. & Buchmann, A. J. *Phys. Rev. C* **64**, 035203 (2001).

39. M. Fiolhais, B. G. & Sirca, S. *Phys. Lett. B* **373**, 229 (1996).

40. Pascalutsa, V. & Vanderhaeghen, M. *Phys. Rev. D* **73**, 034003 (2006).

41. Gail, T. A. & Hemmert, T. R. *Eur. Phys. J A* **28**, 91 (2006).

42. Sanctis, M. D. *et al. Nucl. Phys. A* **755**, 294 (2005).

43. Mandeville, J. *et al. Phys. Rev. Lett.* **72**, 3325 (1994).

44. Drechsel, D., Hanstein, O., Kamalov, S. S. & Tiator, L. A Unitary isobar model for pion photoproduction and electroproduction on the proton up to 1-GeV. *Nucl. Phys.* **A645**, 145–174 (1999).

45. Arndt, R. A., Briscoe, W. J., Strakovsky, I. I. & Workman, R. L. Analysis of pion photoproduction data. *Phys. Rev.* **C66**, 055213 (2002).

46. Pascalutsa, V. & Vanderhaeghen, M. *Phys. Rev. D* **76**, 111501 (2007).

47. Segovia, J. *et al. Few-Body Syst.* **55**, 1185–1222 (2014).

48. Tiator, L. *et al. Eur. Phys. J. A* **17**, 357 (2003).

49. Isgur, N. & Karl, G. *Phys. Rev. D* **18**, 4187 (1978).

50. Rujula, A. D., Georgi, H. & Glashow, S. L. *Phys. Rev. D* **12**, 147 (1975).

51. Rujula, A. D., Georgi, H. & Glashow, S. L. *Phys. Rev. D* **21**, 1868 (1980).

52. Isgur, N., Karl, G. & Koniuk, R. *Phys. Rev. D* **25**, 2394 (1982).

53. Kaelbermann, G. & Eisenberg, J. M. *Phys. Rev. D* **28**, 71 (1983).

54. K. Bermuth, L. T., D. Drechsel & Seaborn, J. B. *Phys. Rev. D* **37**, 89 (1988).

55. Wirzba, A. & Weise, W. *Phys. Lett. B* **188**, 6 (1987).

56. Walliser, H. & Holzwarth, G. *Z. Phys. A* **357**, 317 (1997).

57. Watabe, T., Christov, C. V. & Goeke, K. *Phys. Lett. B* **349**, 197 (1995).

58. Buchmann, A. J., Hernandez, E. & Faessler, A. *Phys. Rev. C* **55**, 448 (1997).

59. 't Hooft, G. *Nucl. Phys. B* **72**, 461 (1974).

60. Witten, E. *Nucl. Phys. B* **160**, 57 (1979).

61. Jenkins, E. *Ann. Rev. Nucl. Part. Sci.* **48**, 81 (1998).

62. Jenkins, E. *Czech. J. Phys.*. **49**, 1273 (1999).

63. Jenkins, E. & Manohar, A. V. *Phys. Lett. B* **335**, 452 (1994).

64. E. Jenkins, X. d. J. & Manohar, A. V. *Phys. Rev. Lett.* **89**, 242001 (2002).

65. A. J. Buchmann, J. A. H. & Lebed, R. F. *Phys. Rev. D* **66**, 056002 (2002).

66. Pascalutsa, V. & Vanderhaeghen, M. *Phys. Rev. D* **76**, 111501 (2007).

67. Grabmayr, P. & Buchmann, A. J. Moments of the neutron charge form-factor and the N —> Δ quadrupole transition. *Phys. Rev. Lett.* **86**, 2237–2240 (2001).

68. Alexandrou, C. *et al. Phys. Rev. D* **83**, 014501 (2011).

69. Alexandrou, C. University of Cyprus, Extended Twisted Mass Collaboration, private communication (2022).

70. Alexandrou, C. *et al. arXiv:2112.04146* (2011).

71. Alexandrou, C. *et al. Phys. Rev. D* **98**, 074502 (2018).

72. Alexandrou, C. *et al. Phys. Rev. D* **66**, 094503 (2002).

73. Alexandrou, C. *et al. Phys. Rev. D* **79**, 014507 (2009).

74. M. N. Butler, M. J. S. & Springer, R. P. *Phys. Lett. B* **304**, 353 (1993).

75. G. C. Gellas, C. N. K., T. R. Hemmert & Poulis, G. I. *Phys. Rev. D* **60**, 054022 (1999).

76. Gail, T. A. & Hemmert, T. R. *Eur. Phys. J. A* **28**, 91 (2006).

77. Pascalutsa, V. & Phillips, D. R. *Phys. Rev. C* **67**, 055202 (2003).

78. Pascalutsa, V. & Vanderhaeghen, M. *Phys. Rev. Lett.* **95**, 232001 (2005).

79. Carlson, C. & Vanderhaeghen, M. *Phys. Rev. Lett.* **100**, 032004 (2008).

80. Fonvieille, H., Pasquini, B. & Sparveris, N. *Prog. Part. Nucl. Phys.* **113**, 103754 (2020).

81. Li, R. *et al. Nature* **611**, 265 (2022).

82. Pasquini, B. *et al. Phys. Rev. C.* **62**, 052201(R) (2000).

83. Pasquini, B., Gorchtein, Drechsel, D., Metz, A. & Vanderhaeghen, M. *Eur. Phys. J. A* **11**, 185 (2001).

84. Drechsel, D., Pasquini, B. & Vanderhaeghen, M. *Phys. Rep.* **378**, 99 (2003).

85. Nakamura, S. *et al. Rep. Prog. Phys.* **80**, 056301 (2017).

86. Nakamura, S., Kamano, H. & Sato, T. *Phys. Rev. D* **92**, 074024 (2015).

87. Atac, H. *et al.* Measurement of the neutron charge radius and the role of its constituents. *Nature Communications* **12**, 1759 (2021).

88. Fernando, I. & Goity, J. *Phys. Rev. D* **101**, 054026 (2020).

89. PR12-09-003: Nucleon Resonance Studies with CLAS12. http://www.jlab.org/exp_prog/proposals/09/PR12-09-003.pdf.

90. PR12-09-003: Proposal Supplement to Nucleon Resonance Studies with CLAS12. https://www.jlab.org/exp_prog/proposals/proposal_updates/PR12-09-003_pac35.pdf.

91. PR12-12-006: Near Threshold Electroproduction of J/ψ at 11GeV. http://www.jlab.org/exp_prog/proposals/12/PR12-12-006.pdf.